Molecular dynamics simulations of the aqueous interface with the [BMI][PF_6] ionic liquid: comparison of different solvent models†‡

G. Chevrot, R. Schurhammer and G. Wipff*

Received 9th June 2006, Accepted 14th July 2006
First published as an Advance Article on the web 3rd August 2006
DOI: 10.1039/b608218a

We report a Molecular Dynamics (MD) study of the interface between water and the hygroscopic room temperature Ionic Liquid "IL" [BMI][PF_6] (1-butyl-3-methyl-imidazolium hexafluorophosphate), comparing the TIP3P, SPC/E and TIP5P models for water and two IL models where the ions are ±1 or ±0.9 charged. A recent MD study (A. Chaumont, R. Schurhammer and G. Wipff, *J. Phys. Chem. B*, 2005, **109**, 18964) showed that using TIP3P water in conjunction with the $IL^{\pm1}$ model led to water–IL mixing without forming an interface, whereas a biphasic system could be obtained with the $IL^{\pm0.9}$ model. With the TIP5P and SPC/E models, the juxtaposed aqueous and IL phases are found to remain distinct for at least 20 ns. The resulting IL humidity, exaggerated with the $IL^{\pm1}$ model, is in better agreement with experiment using the $IL^{\pm0.9}$ model. We also report demixing simulations on the "randomly mixed" liquids, using the $IL^{\pm0.9}$ model for the ionic liquid. With the three tested water models, the phases separate very slowly (≈20 ns or more) compared to "classical" chloroform–water mixtures (less than 1 ns), leading to biphasic systems similar to those obtained after equilibration of the juxtaposed liquids. The characteristics of the interface (size, polarity, ion orientation, electrostatic potential) are compared with the different models. Possible reasons why, among the three tested water models, the widely-used TIP3P model exaggerates the inter-solvent mixing, are analyzed. The difficulty in computationally and experimentally equilibrating water–IL mixtures is attributed to the slow dynamics and micro-heterogeneity of the IL and to the different states of water in the IL phase.

Introduction

Room-temperature ionic liquids (ILs) are generally composed of organic cations (*e.g.* ammonium, imidazolium, phosphonium, pyridinium) and anions[1,2] whose nature largely determines the IL properties [3–8] and, in particular, the macroscopic nature of mixtures with water. For instance, ILs based on hydrophilic anions like Cl^- or BF_4^- are miscible with water, but those containing the hydrophobic PF_6^- or Tf_2N^- anions (Fig. 1) are not. This feature can be exploited for liquid–liquid separation purposes, generally achieved with higher efficiency compared to traditional organic liquids, thereby providing promising "green perspectives" related to the unique solvation and physical properties of the ILs (non volatile, stable, easily tunable, with large electrochemical windows).[9–14] The imidazolium-based hydrophobic ILs are quite commonly used and, like traditional hydrophobic liquids, form a macroscopic "interface" with water. Its microscopic nature is, however, so far poorly understood. As charge–dipole interactions are generally stronger than dipole–dipole interactions, the IL ions interact more strongly with water than do organic molecules (*e.g.* hydrocarbon derivatives, aromatic solvents), perhaps also modifying the properties of the interface. Another distinguishing feature of ILs is their hygroscopic character [15–17] and, depending on the IL constitution, the interface can be expected to evolve from an abrupt and molecularly-sharp zone, as in the case of traditional liquids,[18] to a broader interfacial domain of mixed liquids in gradient concentrations. It is important to understand the interfacial properties of the ILs, which play a key role in fundamental processes like phase transfer catalysis, liquid–liquid extraction and separation processes.

Molecular dynamics (MD) simulations contribute to our understanding of the microscopic nature of interfaces,[18] but publications with ILs are still scarce. Most simulations focused on pure IL properties,[19–23] or their solvation properties towards ionic[24–29] or neutral[30,31] solutes, or their mixtures with liquids like water[30,32,33] or CO_2.[34] A few studies dealt with the IL–gas interface,[35–37] or the disruption of the aqueous "interface" formed by the dimethylimidazolium chloride IL.[38] Our

BMI^+ : R = C_4H_9 1-butyl-3-methyl-imidazolium
OMI^+ : R = C_8H_{17} 1-octyl-3-methyl-imidazolium
PF_6^- Hexafluorophosphate
Tf_2N^- Bis(trifluoromethylsulfonyl)imide

Fig. 1 The BMI^+, OMI^+, PF_6^- and Tf_2N^- ions.

Laboratoire MSM, UMR CNRS 7177, Institut de Chimie, 4 rue B. Pascal, 67 000 Strasbourg, France. E-mail: wipff@chimie.u-strasbg.fr
† The HTML version of this article has been enhanced with additional colour images.
‡ Electronic supplementary information (ESI) available: Table S1 and Fig. S1–S10. See DOI: 10.1039/b608218a

group simulated the aqueous interface with imidazolium-based [BMI][PF_6] and [OMI][PF_6] ILs with a common PF_6^- anion[39,40] and, more recently, the [BMI][Tf_2N] interface with a more hydrophobic anion (acronyms are defined in Fig. 1).[41] These studies employed the TIP3P model for water, and it was found that in the case of the [BMI][PF_6] IL represented with a "primitive" model (denoted $IL^{\pm1}$ *i.e.* with ±1 charged ions), the juxtaposed liquids slowly mixed during the dynamics without forming an interface. A biphasic system could be obtained, however, by turning the IL more hydrophobic, *i.e.* by reducing its ion charges to ±0.9 ($IL^{\pm0.9}$ model), which mimics the anion-to-cation charge transfer.[21] To our knowledge, no comparison of water models has been achieved so far and, as a first step, we decided to consider the [BMI][PF_6]–water binary system and to compare three widely used models based on a 1-6-12 representation of non-bonded interactions, namely, the three points TIP3P[42] and SPC/E[43] models and the more computationally demanding five points TIP5P[44,45] model. The main characteristics of these models are reported in Fig. S1‡. The water–IL system will be simulated starting from juxtaposed solvent boxes of water and IL, in order to investigate whether the liquids mix or form a biphasic system and, if the latter, how does the inter-solvent mixing compare with experiment. The resulting characteristics of the interface, when formed, will be compared. Equilibration of these systems is a difficult task, both experimentally and computationally. As such, we will also consider the time evolution of "randomly mixed" liquids to determine to what extent they separate, and compare the results with those obtained after the simulations at Preformed Interfaces (PI). For convenience, we denote the water–IL systems by their models, *e.g.* $IL^{\pm0.9}$/TIP5P or $IL^{\pm1}$/SPCE; the "PI" simulations start with a Preformed Interface, and the "DE" demixing simulations start with randomly mixed liquids.

Methods

MD simulations have been performed with the AMBER 7.0[46] software with the following representation of the potential energy U:

$$U = \sum_{\text{bonds}} k_1(l-l_0)^2 + \sum_{\text{angles}} k_\theta(\theta-\theta_0)^2 + \sum_{\text{dihedrals}}\sum_{n} V_n(1+\cos(n\varphi-\gamma)) + \sum_{i<j}\left[\frac{q_iq_j}{R_{ij}} - 2\varepsilon_{ij}\left(\frac{R^*_{ij}}{R_{ij}}\right)^6 + \varepsilon_{ij}\left(\frac{R^*_{ij}}{R_{ij}}\right)^{12}\right]$$

It accounts for the deformation of bonds, angles, dihedral angles, electrostatic and van der Waals 1-6-12 interactions. Non-bonded interactions were calculated with a 12 Å atom-based cutoff, correcting for the long-range electrostatics by using the Ewald summation method (PME approximation[47]). The solutions were simulated with 3D-periodic boundary conditions. The solvents were represented explicitly at the molecular level with the TIP3P[42], TIP5P[44,45] or SPC/E[43] models for water, with the OPLS[48] model for PF_6^- anions and with parameters of reference[49] for BMI^+ cations. Two electrostatic models were used for the IL ions: the "standard" model with ±1 charged ions, denoted $IL^{\pm1}$, and a "scaled" model with ±0.9 charged ions, denoted $IL^{\pm0.9}$. The corresponding atomic charges and AMBER atom types are given in Fig. S1‡. Cross terms in van der Waals interactions were constructed using the Lorentz–Berthelot rules. The 1–4 van der Waals interactions and the 1–4 electrostatic interactions were scaled down by 2.0 and 1.2, respectively as recommended by Cornell *et al.*[50] The interface was built from adjacent boxes of water and IL, containing 2119 H_2O and 181 BMI^+ PF_6^- molecules, respectively. The resulting box size is 40 × 40 × 80 $Å^3$. After 1000 steps of energy minimization (100 steps by the steepest descent and 900 steps by conjugate gradients), we performed 150 ps of dynamics at 300 K at a pressure of 1 atm, followed by a production step at constant volume. The temperature was kept constant by coupling the solution to a thermal bath using the Berendsen algorithm[51] with a relaxation time of 0.2 ps. In the case of (NPT) simulations at constant pressure, the pressure was similarly coupled to a barostat[51] with a relaxation time of 0.2 ps. All C–H bonds were constrained with SHAKE,[52] using a time step of 2 fs to integrate the equation of motion.

Mixing–demixing MD simulations were performed on [BMI][PF_6]–water mixtures. The mixing stage started after *ca.* 10 ns of dynamics at the PI and was achieved by running 1 ns of dynamics at 600 K with biased potentials (electrostatics scaled down by using a dielectric constant of 100). The subsequent DE simulations were performed at a temperature of 300 K, resetting the dielectric constant to 1.

The trajectories were saved every ps and analyzed by visual inspection at the computer graphics systems and using our MDS software.[53] The snapshots presented here were redrawn with the VMD software.[54] The densities of water and of the IL were calculated as a function of the z-coordinate in slices of Δz = 0.5 Å width and the position of the interface (z = 0) was dynamically defined by the intersection of the water and IL density curves, calculated from all atoms present in the Δz slice. In order to be able to compare one system to the other or to describe the time evolution of a given system, we decided to define the "frontier" between the "bulk" liquid and interfacial domains at z = ±12 Å, which is generally somewhat more than half of the interfacial width (*vide infra*). The amount of IL in bulk water was estimated as an average of the XMI^+ and PF_6^- contributions, selecting the center of mass of the ions to

Table 1 Characteristics of the simulated water–IL systems

	Time/ns
Preformed interface[a]	
$IL^{\pm1}$/SPC/E PI	20
$IL^{\pm1}$/TIP5P PI	21
$IL^{\pm0.9}$/TIP3P PI	20
$IL^{\pm0.9}$/SPC/E PI	30
$IL^{\pm0.9}$/TIP5P PI	25
Mixed system[b]	
$IL^{\pm0.9}$/TIP3P DE	21
$IL^{\pm0.9}$/SPC/E DE	40
$IL^{\pm0.9}$/TIP5P DE	25

[a] PI: Simulation starting at a preformed interface. [b] DE: Demixing simulation.

define their position. The electrostatic potential $\phi(z)$ was calculated with a 12 Å cutoff + PME correction during the last ns. $\phi(z)$ was obtained in xy slices of $\Delta z = 0.5$ Å thickness, as an average over 5×5 grids of about 64 Å^2 each, including the contributions of all ions and solvent atoms of the simulated box or of its nearest periodic image. The diffusion coefficients D were calculated with the Einstein relation: $D = \frac{1}{6} \lim_{t\to\infty} \frac{d}{dt} \left\langle |r_i(t) - r_i(0)|^2 \right\rangle$, and averaged for 0.5 ns for all molecules that reside in a given domain during that time.

Results

Water–IL mixing, obtained from juxtaposed *versus* mixed liquids

In this section, we first examine the evolution of a biphasic water–IL system built from adjacent liquids (PI simulations), with the main aim to test the different models to discover whether the phases remain separated to form an interface or mix during the dynamics. Furthermore, the extent of solvent mixing in the simulation will be compared with experiment and characterized by the molar fraction of IL in water (hereafter denoted x_{IL}) and of the molar fraction of water in the IL (hereafter denoted x_{wat}). There are different experimental values of x_{IL} and x_{wat} (Table 2), depending of the IL purity and working conditions, and we will take the values of Anthony *et al.*[15] ($x_{IL} \approx 1.3 \times 10^{-3}$ and $x_{wat} \approx 0.26$) for the [BMI][PF_6] IL for reference. These values were obtained at a controlled temperature of 22 °C, after extensive stirring (24 or 48 h), followed by 1 to 2 hours of decantation. They are close to those obtained by Luo *et al.*[55] after 1 h of shaking. Higher x_{wat} values correspond either to more extensive mixing ($x_{wat} = 0.30$ in ref. 56) or possibly to impurities ($x_{wat} = 0.68$ in ref. 57). Note that for x_{IL}, the comparisons with simulation results can be only qualitative, for several reasons. At the macroscopic scale, each phase is electrically neutral, while in the calculations (''nano solution''), one may find some excess of IL anions over cations in ''bulk'' water (*vide infra*), and x_{IL} is calculated from the average of the cation and anion contributions. Second, the number of IL ions in water is small and fluctuates with time (Fig. S7‡), leading to poor statistics. Also, note the somewhat arbitrary definition of the ''interfacial'' and ''bulk'' liquid domains, which are less well separated with the IL than with classical liquids. Due to computer time limitations, the dynamics were generally stopped when the calculated value of x_{wat} clearly exceeded the experimental ones. Furthermore, we did not recalculate the $IL^{\pm1}$/TIP3P system that has been found to mix.[39] Typical snapshots at the end of the dynamics can be seen in Fig. 2, S2‡ and S3‡, and the time evolution of the x_{IL} and x_{wat} is presented in Fig. 3 and S6‡. The IL and water density curves are also represented in Fig. S3‡. The final x_{IL} and x_{wat} values are collected in Table 3.

The two simulations with the $IL^{\pm1}$ model were thus performed in conjunction with the SPC/E and TIP5P water models, yielding significantly different results. The $IL^{\pm1}$/SPCE system did not stabilize during the simulated 20 ns, as the liquids continuously mixed, finally reaching molar fractions x_{wat} and x_{IL} of *ca.* 0.6 and 0.02, respectively, which are too high compared to experiment. With TIP5P water, the system reaches an equilibrium at *ca.* 12 ns, with x_{wat} displaying a plateau until the end of the dynamics (20 ns). The IL phase is, however, too humid ($x_{wat} \approx 0.4$) and there is too much IL in water ($x_{IL} \approx 0.004$).

As expected, when the ionic liquid is represented with the lower charged $IL^{\pm0.9}$ model, it mixes less with water and somewhat different results are obtained, depending on the water model. With TIP3P water, the IL humidity is ''rapidly'' stabilized (in *ca.* 5 ns), leading to a molar fraction x_{wat} of $\approx$0.6, higher than experiment. The x_{IL} value of $\approx$0.008 is also too high. The IL ions seem to be more hydrophobic with the TIP5P than with the TIP3P water, because the former model yields less inter-solvent mixing: $x_{wat} \approx 0.3$ and $x_{IL} \approx 0.001$. Note that with this $IL^{\pm0.9}$/TIP5P model, the x_{wat} amount of water in the IL is not constant but oscillates between 0.2 and 0.3 in the 10 to 25 ns time period. With the SPC/E water model, the IL humidity does not change regularly with time: x_{wat} amounts to $\approx$0.15 after 15 ns, to $\approx$0.29 at 22 ns, and to $\approx$0.20 between 25 and 30 ns. These values are closer to those obtained with the TIP5P, than with the TIP3P water. Thus, the TIP5P and SPC/E water models, used in conjunction with the $IL^{\pm0.9}$ ionic liquid model, bracket the experimental value of water in the saturated IL, whereas TIP3P water mixes too much with the ionic liquid.

The outcome of phase separation was investigated, selecting for the IL model that did not exaggerate the miscibility with water, *i.e.* the $IL^{\pm0.9}$ model and the three water models. Typical snapshots along the dynamics can be seen in Fig. S4‡ and S5‡, and the time evolution of the demixing index $\chi(t)$ is shown in Fig. 4. Initially, the liquids were completely mixed ($\chi \approx 0.8$) and remained so at 1 ns, which is about the time after which similar water mixtures with classical liquids are fully separated.[58] After 10 ns, one sees water rich domains and IL rich domains, but still no well-defined interface between water and the [BMI][PF_6] phase. The demixing index χ at that time is

Table 2 Literature values of the molar fractions of water in [BMI][PF_6] (x_{wat}) and of [BMI][PF_6] in water (x_{IL})

	x_{wat}	x_{IL}
Carda-Broch *et al.*, *Anal. Bioanal. Chem.*, 2003, **375**, 191	0.21	0.00113
Anthony *et al.*, *J. Phys. Chem. B*, 2001, **105**, 10942	0.26	0.00129
Huddleston *et al.*, *Green Chemistry*, 2001, **3**, 156	0.16	—
Luo *et al.*, *Anal. Chem.*, 2004, **76**, 2773	0.25	0.0016
Visser *et al.*, *Ind. Eng. Chem. Res.*, 2000, **39**, 3596	0.21	—
Chun *et al.*, *Anal. Chem.*, 2001, **73**, 3737	—	0.0012
Schröder *et al.*, *New J. Chem.*, 2000, **24**, 1009	0.68	—
Jacquemin *et al.*, *Green Chem.*, 2006, **8**, 172	0.30	—
Luo *et al.*, *Solvent Extraction Ion Exchange*, 2006, **24**, 19	0.25	0.0016

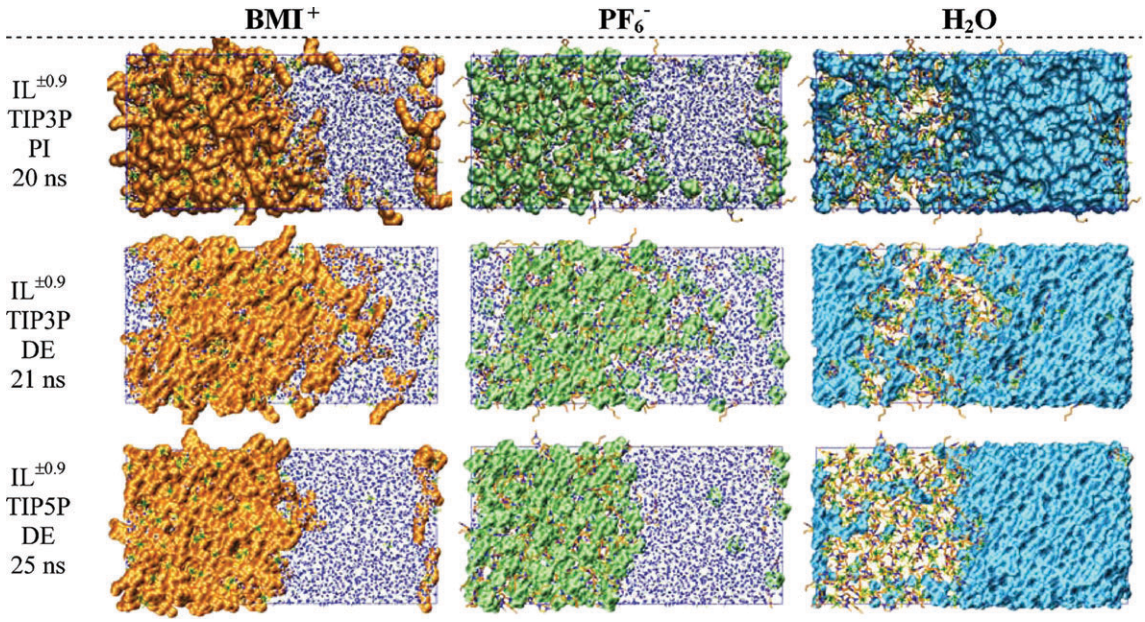

Fig. 2 Snapshots at selected water–IL mixtures from MD simulations at PI and from the DE simulation, showing separately, from left to right: the BMI^+ cations (orange), the PF_6^- anions (green) and water (blue). A full version of the figure and corresponding density curves are given in Fig. S2‡ and S3‡.

ca. 0.6 with TIP3P water, 0.5 with SPC/E water and 0.4 with TIP5P water, indicating that the rate of the phase separation increases in this series. At 20 ns, the two phases are quite apparent and delineate an interface, and the humidity of the ionic liquid phase amounts to $x_{wat} \approx 0.25$ with TIP5P water, and to $\approx$0.6 with SPC/E water. These values are comparable to, but somewhat higher than those found when the liquids were initially juxtaposed. The dynamics with SPC/E water was pursued up to 40 ns, showing further phase separation and water diffusion from the IL to the aqueous phase. The final x_{wat} value of $\approx$0.3 is higher than the final value obtained at the preformed interface (0.23), and also close to experiment. The DE simulation with TIP3P water also leads to incomplete phase separation after *ca*. 20 ns, without forming a well-defined interface, and the resulting x_{wat} and x_{IL} values (0.71 and 0.009, respectively) are higher than with the TIP5P or SPC/E water models. This simulation with TIP3P water has not been pursued any further because the mixing at the preformed interface is too high. Thus, the three studied water models, combined with the $IL^{\pm 0.9}$ ionic liquid model, lead to two more or less separated phases as do juxtaposed liquids, but inter-solvent mixing is exaggerated with TIP3P water. The

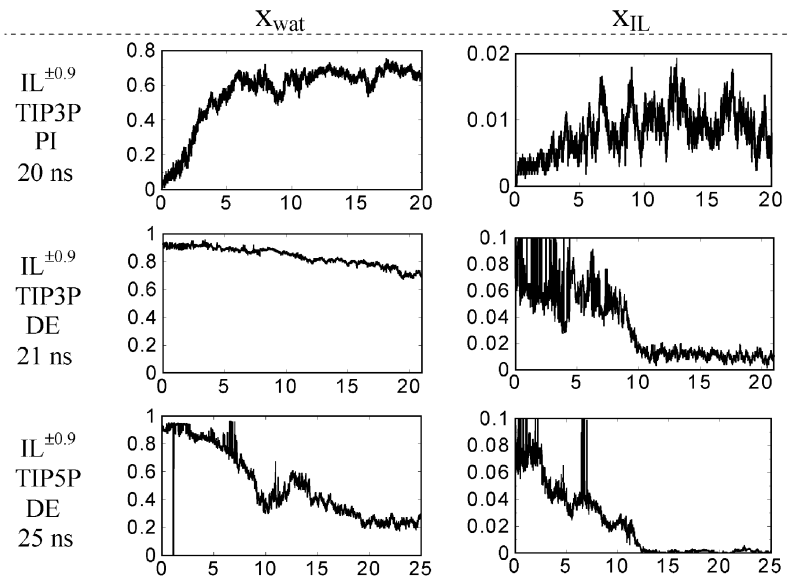

Fig. 3 Molar fraction of water in IL (x_{H_2O}) and molar fraction of IL in water (x_{IL}) as a function of time (ns). A full version is given in Fig. S6‡ and the detailed contributions of BMI^+ and PF_6^- ions in water are shown in Fig. S7‡.

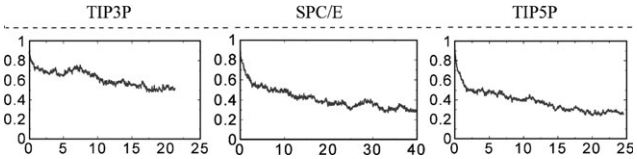

Fig. 4 Demixing index χ ($1/\chi = 1/d_{water} + 1/d_{IL}$) as a function of time (ns) for the water–$IL^{\pm 0.9}$mixtures with the three water models. d_{water} is the local density of water and d_{IL} is the local density of the IL, as defined in ref. 58.

characteristics of their interfaces are discussed below in more detail.

Characteristics of the aqueous interface of [BMI][PF_6] ionic liquid. Comparison of different solvent models

In this section, we focus on the interface, calculated using the different models. As the extent of solvent mixing depends on the solvent model, it is important to assess to what extent the interface changes. We thus analyze the interface width, the orientation of cations at the interface, and the evolution of electrostatic potentials in the *z*-direction, which directly reflects the charge distribution as one moves from the bulk IL to the bulk water phase. Unless otherwise specified, we consider the interfaces obtained from juxtaposed liquids.

Shape and width of the interface. The definition of the interfacial width is somewhat arbitrary and, as in ref. 39, was defined as the *z*-distance between the points where the solvent densities reach 90% of their "bulk" experimental values, averaging over the two equivalent water–IL interfaces. The results are collected in Table 3. For PI, the interface width decreases in the order: $IL^{\pm 1}$/TIP3P (mixed) > $IL^{\pm 1}$/SPCE (mixed) > $IL^{\pm 0.9}$/TIP3P (≈18.9 Å) > $IL^{\pm 1}$/TIP5P (≈14.3 Å) > $IL^{\pm 0.9}$/SPCE (≈10.9 Å) > $IL^{\pm 0.9}$/TIP5P (≈9.3 Å). Similar values are obtained after the DE simulations, yielding the same sequence for the studied systems: $IL^{\pm 0.9}$/TIP3P (≈22.1 Å) > $IL^{\pm 0.9}$/SPCE (≈10.6 Å) > $IL^{\pm 0.9}$/TIP5P (≈9.4 Å). This follows the trends in inter-solvent mixing described above, showing that the interface becomes narrower when the IL ions get less charged, and when one replaces the TIP3P water by the other models. The TIP5P interface, where the x_{IL} amount is the smallest, is also the narrowest. Note, the latter is, however, wider than the classical chloroform–water interface (≈7 Å).[59]

Table 3 Molar fraction of water in the IL and of the IL in water (averages over the last ns), and width of the interface

	x_{wat}	x_{IL}	Width/Å
Preformed interface $IL^{\pm 1}$ [a]			
$IL^{\pm 1}$/SPC/E PI	0.65	0.023	—
$IL^{\pm 1}$/TIP5P PI	0.45	0.004	14.3
Preformed interface $IL^{\pm 0.9}$ [a]			
$IL^{\pm 0.9}$/TIP3P PI	0.66	0.008	18.9
$IL^{\pm 0.9}$/SPC/E PI	0.23	0.004	10.9
$IL^{\pm 0.9}$/TIP5P PI	0.27	0.001	9.3
Demixing simulation $IL^{\pm 0.9}$ [b]			
$IL^{\pm 0.9}$/TIP3P DE	0.71	0.009	22.1
$IL^{\pm 0.9}$/SPC/E DE	0.29	0.002	10.6
$IL^{\pm 0.9}$/TIP5P DE	0.25	0.001	9.4

[a] PI: Simulation starting at a preformed interface. [b] DE: Demixing simulation.

Typical snapshots (Fig. 2 and S2‡) reveal that the interfaces are quite rough, even in the case of the $IL^{\pm 0.9}$/TIP5P system, for which the interface is narrowest (Table 3). Interestingly, at that interface, one finds cations and anions of IL that are fully surrounded by water, thus without contact with the bulk IL phase and, similarly, water molecules isolated from the bulk water, solvated by IL ions. Such patterns are amplified with the other models based on more miscible liquids, and differ markedly from the classical interfaces where the molecules of a given liquid always retain direct connections with their bulk phase.

Orientation of imidazolium cations at the interface. The BMI^+ cations display an amphiphilic topology (apolar butyl chain and charged imidazolium head) and might adopt specific orientations at the interface, as found for their analogues with longer chains.[39] In order to analyze this feature with the different systems, we defined the angle θ between the *z*-axis of the box and the N–C vector connecting the N_2 atom and the terminal carbon of the alkyl chain, and compared the orientations of BMI^+ cations as a function of their *z*-position. The corresponding order parameter *S*, defined by $S = 0.5 \langle 3\cos^2\theta - 1\rangle$ would range from −0.5 (if the cations were perfectly ordered parallel to the interface) to 1.0 (if they were perpendicular). In fact, all average *S* values are close to zero (lower than 0.1 in magnitude) at the interface and in the bulk IL (Fig. 5 and S8‡), indicating that the BMI^+ cations are isotropically oriented in the different portions of the solution and at the interface with the various models.

Polarity of the interface. A previous report using the $IL^{\pm 0.9}$/TIP3P model indicated that the solvent distribution leads to an electrostatic potential $\phi(z)$ that changes with the distance from the interface.[39] The potential arises from both short and long range contributions and thus from the treatments of electrostatics. The results, obtained using a consistent methodology for the three water–$IL^{\pm 0.9}$models and two water–$IL^{\pm 1}$ models are plotted in Fig. S9‡. They show that $\phi(z)$ is very similar with all models, *i.e.* negative on the water side and positive on the IL side of the solution. The potential $\phi(z)$ results from the IL and water contributions, *i.e.* from the representation of these liquids. The resulting $\phi(z)^{IL}$ and $\phi(z)^{wat}$ distributions are found to be antagonistic, and to depend on the water model. With the SPC/E and TIP3P water, the $\phi(z)^{wat}$ component is negative on the water side, and positive on the IL side of the interface, while with the TIP5P water, the trend is reversed. The IL model has little effect on the distribution of the potentials. In the case of TIP5P water, the negative potential in water may stem from the small excess of PF_6^- over BMI^+ ions in water, as seen from the analysis reported in Fig. S7‡. With the two other water models, there are similar concentrations of cations and anions in water.

Further insights into the role of water on the interfacial potential can be obtained by analyzing the total *z*-component μ_z of the $\mu(H_2O)$ dipoles as a function of the *z*-position in the solution showing two types of behaviour (Fig. S10‡),

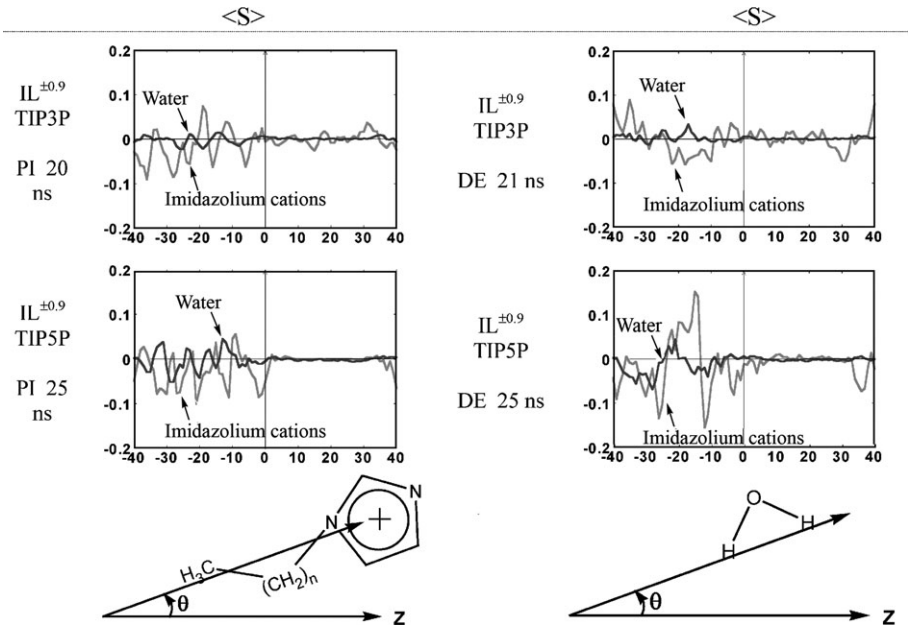

Fig. 5 Order parameter S of imidazolium cations and water molecules, as a function of their z-position (averages over the last 3 ns). Angle θ between the z-axis and the N_2-CH_3 vector of the alkyl chain of BMI^+, or the H–H vector of the H_2O molecules. A full version of the figure is given in Fig. S8‡.

depending on the water model. With the TIP5P water, the μ_z dipole is positive and maximum at the interface and decreases to zero in bulk water, whereas with the SPC/E and TIP3P water models, μ_z is negative and minimum at the interface. These features are observed with the $IL^{\pm 0.9}$ as well as with the $IL^{\pm 1}$ models of ionic liquid. This analysis thus shows that the similarity in interfacial potential $\phi(z)$ in fact hides a complex interplay between the model-dependent IL ions and water distributions, and the resulting electrostatic contributions.

Discussion and conclusions

We reported MD investigations on the interface between the hydrophobic, but hygroscopic, [BMI][PF_6] IL and water, comparing three water models (TIP3P *vs.* TIP5P *vs.* SPC/E) and two IL models ($IL^{\pm 0.9}$ *vs.* $IL^{\pm 1}$), with the main aim of assessing the extent of inter-solvent mixing, and the nature of the resulting interface. The $IL^{\pm 0.9}$ model is less hydrophilic than the $IL^{\pm 1}$ model and corresponds to the scaling factor of 0.9 used previously to mimic the anion-to-cation charge transfer found by Quantum Mechanical (QM) calculations, while retaining the dominant polar character of the IL.[21,39] Due to the long computing times required, we did not attempt to optimize this factor, but the results clearly demonstrate the importance of the water and IL models on the interface properties. When the IL is represented by its "primitive model" (±1 charged ions), its interactions with water are exaggerated, leading to complete mixing with TIP3P water, and to distinct phases after 20 ns with the SPC/E or TIP5P juxtaposed liquids. The resulting x_{IL} and x_{wat} values are, however, clearly too high and should increase further in the case of the SPC/E interface if the dynamics were extended. Better results are obtained with the less polar $IL^{\pm 0.9}$ model, which interacts less with water, yielding similar x_{IL} and x_{wat} values when used in conjunction with the TIP5P and the SPC/E water models, in close agreement with experiment. With TIP3P water, the miscibilities remain too high. It thus looks as though the water–IL interactions are too attractive with TIP3P water. With regard to the $IL^{\pm 0.9}$ ions solubilized in water, one sees that there is an equal amount of BMI^+ and PF_6^- ions with the TIP3P and SPC/E models, whereas the PF_6^- are in excess with the TIP5P model.

In order to test key interactions involved in the water–IL mixing, we first analyzed water–ion optimized dimers, as well as aqueous solutions of IL ions "at infinite dilution" and "humid" IL, with the different models. The results, summarized in Table 4, show that AMBER binding energies of the $PF_6^-\cdots H_2O$ and $BMI^+\cdots H_2O$ dimers are similar for the two ions, and similar with the three water models: they range from −10.0 to −11.4 kcal mol^{-1} with the $IL^{\pm 1}$ model, and from −8.8 to −10.2 kcal mol^{-1} with the $IL^{\pm 0.9}$ model. They are also

Table 4 Water–ion dimers. Binding energies calculated with AMBER and from BSSE-corrected QM calculations

	$PF_6^-\cdots H_2O$	$BMI^+\cdots H_2O$
HF[a]	−9.1	−9.7
DFT[a]	−9.5	−9.5
AMBER (TIP3P)	−11.5	−10.2
AMBER (TIP5P)	−10.5	−10.3
AMBER (SPC/E)	−11.4	−10.0
	$\mathbf{PF_6^{-0.9}\cdots H_2O}$	$\mathbf{BMI^{+0.9}\cdots H_2O}$
AMBER (TIP3P)	−10.2	−8.8
AMBER (TIP5P)	−9.3	−9.3
AMBER (SPC/E)	−10.1	−9.1

[a] From A. Chaumont and G. Wipff, *Inorg. Chem.*, 2004, **43**, 5891.

Table 5 Average interaction energies (in kcal mol^{-1}) of one ion pair with all water,[a] of one water molecule with all IL ions,[b, c] averaged over all H_2Os from the mixture[c]

	One ion pair in bulk water [a]		One H_2O in bulk $IL^{\pm0.9}$ [b]		One H_2O in bulk $IL^{\pm1}$ [b]		Humid $IL^{\pm0.9}$ [c]	
	$BMI^{+0.9}$	$PF_6^{-0.9}$	$BMI^{+0.9}$	$PF_6^{-0.9}$	BMI^{+1}	PF_6^{-1}	$BMI^{+0.9}$	$PF_6^{-0.9}$
Water TIP3P	-64 ± 6	-96 ± 7	-5 ± 2	-10 ± 2	—	—	−3.1	−7.4
Water TIP5P	-74 ± 6	-84 ± 7	-6 ± 2	-6 ± 2	-3 ± 2	-8 ± 3	−4.0[d]	−6.1[d]
Water SPC/E	-65 ± 5	-98 ± 7	-6 ± 2	-8 ± 2	-4 ± 2	-10 ± 3	—	—

MD simulations of:[a] 1 BMI^+, PF_6^- ion pair in water. [b] 1 H_2O in bulk IL. [c] "Humid" IL (with a 1 : 3 ratio of water : IL, *i.e.* with 573 ion pairs plus 191 H_2O molecules). [d] The TIP5P energies have been calculated based on the configurations generated with the TIP3P model.

close to the QM calculated values (≈ -10 kcal mol^{-1} at the HF or DFT levels with BSSE correction). Looking more precisely at the small differences shows that the AMBER interactions with PF_6^- follow the order TIP3P $\approx$ SPC/E > TIP5P with the two IL models, while with BMI^+ the order of interactions is: SPC/E < TIP3P < TIP5P ($IL^{\pm1}$ model) and TIP3P < SPC/E < TIP5P ($IL^{\pm0.9}$ model).

As solvation may involve multiple modes of binding and cooperative effects, we also analyzed the water interactions with the IL ions in diluted aqueous solutions, obtained from independent simulations with one separated (at *ca.* 25 Å) ion pair per box of water. The results (Table 5) show that the PF_6^- anion interacts better than the BMI^+ cation with water, by 10 to 30 kcal mol^{-1} depending on the model, presumably due to the larger accessibility of PF_6^- to water compared to the polar C–H protons of BMI^+. Furthermore, the interactions of the anion and of the cation do not follow the same order with the different water models: TIP3P $\approx$ SPC/E > TIP5P for PF_6^- and TIP3P $\approx$ SPC/E < TIP5P for BMI^+. Summing over the two ion contributions yields similar energies (≈ -160 kcal mol^{-1}) with the three water models. There is thus no clear evidence for stronger interactions of the most miscible (TIP3P) water model with the two IL ions, compared to the other models.

The interactions of water with the IL were similarly investigated with selected models based on two types of system. First, a single H_2O molecule in the IL and, second, a "humid" IL, containing a 1 : 3 ratio of H_2O : IL ions, close to the experimental ratio in saturation conditions (Table 2). The results show that a single H_2O molecule diluted in the IL interacts with the latter in the order TIP5P < SPC/E < TIP3P, with different contributions of the anionic and cationic components of the IL depending on the water model. When one moves from the $IL^{\pm1}$ to the $IL^{\pm0.9}$ model, interactions are scaled down as expected, but the order is retained. In the "humid" IL ($IL^{\pm0.9}$ model), we compared the water–IL interaction energies ΔE with the TIP5P and TIP3P models, based on identical configurations (generated with the TIP3P model), and found identical total ΔEs, again due to different contributions of the IL cations and anions (Table 5). Thus, there is again no simple explanation of the higher and exaggerated mixing with TIP3P water, compared to the other models, based on water–ion interactions.

A possible explanation comes from the higher diffusion of TIP3P water compared to the SPC/E or TIP5P water. The average diffusion coefficients D (in 10^{-5} cm^2 s^{-1}) of water in the "bulk" water phase in contact with the $IL^{\pm0.9}$ liquid are: 3.4, 1.6 and 2.1 with the TIP3P, SPC/E and TIP5P models, respectively, in the PI simulations, and 3.1, 1.7 and 2.0 in the DE simulations (Table S1‡). They are smaller than in pure water (5.5, 2.7 and 2.7, respectively, according to independent simulations using the same protocol as for the interfaces, or 5.1, 2.5 and 2.6, respectively, from ref. 45) due to the confinement of water between IL slabs, and the solubilization of IL ions in that domain. These results are consistent with the observations that interfacial and transport properties of TIP3P water obtained with Ewald summation methods are further from experiment than the cut-off based results,[60] *i.e.* obtained using conditions in which the model has been developed.[42] Also, note that with all models studied, the diffusion of H_2O and IL ion molecules increases with the humidity, *i.e.* when one moves from the "bulk" IL to the interface and to bulk water, in agreement with experimental observations.[10,57]

Generally, water is found to exchange from the bulk aqueous phase to the IL phase during the dynamics (see cumulated H_2O positions in Fig. 6), and this process is also model dependent. For instance, at the $IL^{\pm0.9}$ interface, the number of water molecules whose lifetime in the bulk water phase (without exchanging with the IL or the interface) is at least 0.5 ns is only four with TIP3P water, and *ca.* 40 with SPC/E or TIP5P water. The same results are found at the end of the PI or DE simulations (Table S1‡), which indicates that the difference does not stem from insufficient equilibration of the systems. Thus, the properties of the water mixtures with ionic liquids do not only depend on the pair-wise interactions between liquid components, but also on other components (*e.g.* solvophobic interactions, including entropy effects) and on dynamics.

There are different states of water in the IL phase according to spectroscopic investigations[17] and to the simulations. Even in the $IL^{\pm0.9}$-TIP5P system, where intermixing is the least pronounced, one finds in the IL phase, in addition to water monomers, water oligomers. Examination at the graphics system and snapshots (Fig. 7) show that each water proton is typically H-bonded to one PF_6^- anion, whereas the water oxygen points towards C_2H or C_4H aromatic protons of BMI^+ cations in the case of monomers. Water fluctuates in these micro-basins for several hundreds of picoseconds before "jumping" to the next basin (see cumulated trajectories for 1 ns in Fig. 6). Also note that, at longer time periods, water exchanges between the bulk IL and bulk water phases (compare cumulated views for 5 ns in Fig. 6). This does not happen with classical hydrophobic organic solvents. It is interesting to compare two ionic liquids with a same cation (BMI^+) but different anions (PF_6^- *versus* Tf_2N^-), simulated with the same

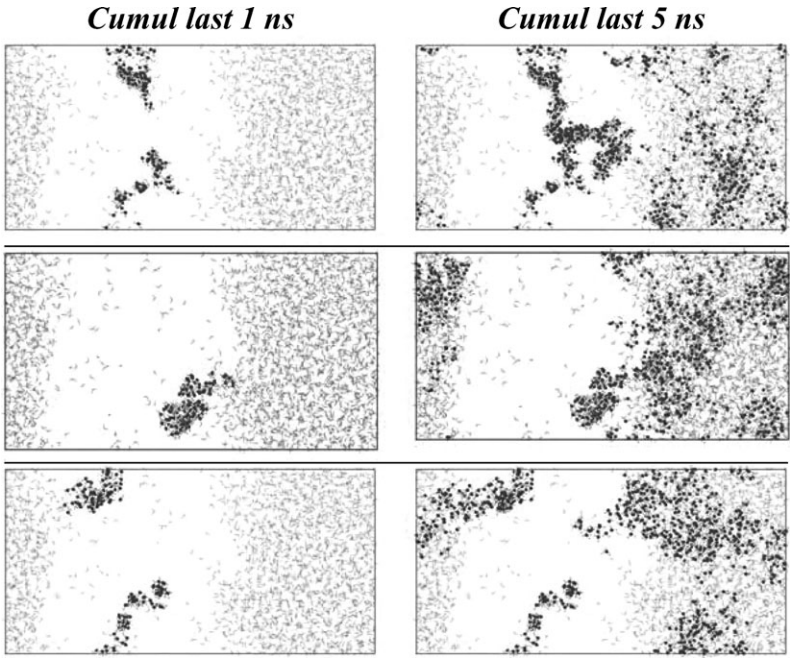

Fig. 6 (a) The $IL^{\pm 0.9}$–TIP5P interface (at 20 ns). Cumulated positions of one selected H_2O molecule in the bulk IL, during the last 1 ns (left) and the last 5 ns (right), every 5 ps. The final configuration of water is faintly superposed. Lines 1–3 correspond to three different water molecules.

models ($IL^{\pm 0.9}$ – TIP3P). Interestingly, the diffusion coefficient of water in the IL phase with $[BMI][PF_6]^{\pm 0.9}$ (this study) is *ca.* twice higher than with the $[BMI][Tf_2N]^{\pm 0.9}$ ionic liquid,[41] presumably because the isotropic charge distribution of the PF_6^- anions provides a better relay to assist the water migration, compared to the amphiphilic Tf_2N^- anion whose H-bonding interactions are more stereochemically demanding. This is also consistent with the fact that the $[BMI][PF_6]$ IL is more hygroscopic than $[BMI][Tf_2N]$, leading to higher diffusion of its components.[10,57]

The different states of water in the IL most likely correspond to different timescales concerning the structure and dynamics of the IL phase, implying temperature-dependent specific equilibration issues. When compared to the binary systems with hydrophobic organic liquids, the water–IL systems separate much more slowly (in *ca.* 20 ns or more in our simulations for the water–IL, and in less than 1 ns for the water–chloroform mixture).[58] We believe that the equilibration problems met with IL's simulations on "nano solutions" reflect those met experimentally. Note the different experimental solubility values reported for the binary system studied (Table 2), likely due to the different protocols and possible impurities in the IL. Similarly, the water solubility in the $[BMI][Tf_2N]$ IL has been reported to range from 0.07[7] to 0.32[56] in molar fraction, probably dependent on the experimental protocol. Surface tension measurements indicate that the surface tension of the biphasic water–$[BMI][Tf_2N]$ system decreases from 15.9 to 13.7 dyne cm^{-1} after several hours when the two purified liquids were placed in contact, illustrating specific issues with the ILs and their interfaces.[61] To our knowledge, there are no such equilibration problems with classical molecular liquids. On the computational side, an important challenge will be to investigate the size dependence of the interfacial system, in conjunction with the representation of the potential energy by more elaborate (*e.g.* polarizable)[36] force fields.

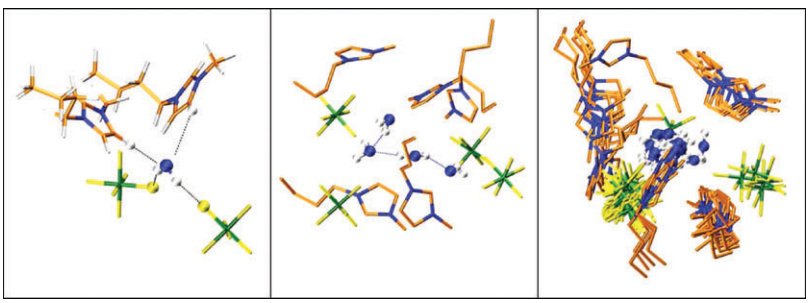

Fig. 7 Snapshots of a water monomer (left) and oligomers (middle) with cumulated positions (right) after 20 ps in the IL phase of the $IL^{\pm 0.9}$–TIP5P interface (at 20 ns).

Acknowledgements

The authors are grateful to IDRIS, CINES, Université Louis Pasteur and to the GDR CNRS-PARIS for computer resources, and to E. Engler and A. Chaumont for assistance. GC thanks the University Louis Pasteur for a PhD grant.

References

1 *Ionic Liquids in Synthesis*, ed. P. Wasserscheid and T. Welton, Wiley-VCH, Weinheim, 2002.
2 F. Endres and S. Z. El Abedin, *Phys. Chem. Chem. Phys.*, 2006, **8**, 2101–2116.
3 J. Dupont and P. A. Z. Suarez, *Phys. Chem. Chem. Phys.*, 2006, **8**, 2441–2452.
4 H. Tokuda, K. Hayamizu, K. Ishii, M. Abu Bin Hasan Susan and M. Watanabe, *J. Phys. Chem. B*, 2004, **108**, 16593–16600.
5 C. P. Fredlake, J. M. Crosthwaite, D. G. Hert, S. N. V. K. Aki and J. F. Brennecke, *J. Chem. Eng. Data*, 2004, **49**, 954–964.
6 N. L. Lancaster and T. Welton, *J. Org. Chem.*, 2004, **69**, 5986–5992.
7 J. G. Huddleston, A. E. Visser, W. M. Reichert, H. D. Willauer, G. A. Broker and R. D. Rogers, *Green Chem.*, 2001, **3**, 156–164.
8 R. Hagiwara and Y. Ito, *J. Fluorine Chem.*, 2000, **105**, 221–227.
9 T. Welton, *Chem. Rev.*, 1999, **99**, 2071–2083.
10 P. A. Z. Suarez, V. M. Selbach, J. E. L. Dullius, S. Einloft, C. M. S. Piatnicki, D. S. Azambuja, R. F. de Souza and J. Dupont, *Electrochim. Acta*, 1997, **42**, 2533–2535.
11 R. D. Rogers and K. R. Seddon, *Science*, 2003, **302**, 792–793.
12 M. J. Earle and K. R. Seddon, *Pure Appl. Chem.*, 2000, **72**, 1391–1398.
13 J. S. Wilkes, *Green Chem.*, 2002, **4**, 73–80.
14 H. L. Ngo, K. LeCompte, L. Hargens and A. B. McEwen, *Thermochim. Acta*, 2000, **357**, 97–102.
15 J. L. Anthony, E. J. Maginn and J. F. Brennecke, *J. Phys. Chem. B*, 2001, **105**, 10942–10949.
16 D. S. H. Wong, J. P. Chen, J. M. Chang and C. H. Chou, *Fluid Phase Equilib.*, 2002, **194–197**, 1089–1095.
17 L. Cammarata, S. G. Kazarian, P. A. Salter and T. Welton, *Phys. Chem. Chem. Phys.*, 2001, **3**, 5192–5200.
18 I. Benjamin, *Chem. Rev.*, 1996, **96**, 1449–1475.
19 S. M. Urahata and M. C. C. Ribeiro, *J. Chem. Phys.*, 2004, **120**, 1855–1863.
20 M. G. Del Popolo and G. A. Voth, *J. Phys. Chem. B*, 2004, **108**, 1744–1752.
21 T. I. Morrow and E. J. Maginn, *J. Phys. Chem. B*, 2002, **106**, 12807–12813.
22 J. N. A. C. Lopes and A. A. H. Padua, *J. Phys. Chem. B*, 2006, **110**, 3330–3335.
23 Y. Wang and G. A. Voth, *J. Am. Chem. Soc.*, 2005, **127**, 12192–12193.
24 A. Chaumont and G. Wipff, *Phys. Chem. Chem. Phys.*, 2003, **5**, 3481–3488.
25 A. Chaumont, E. Engler and G. Wipff, *Inorg. Chem.*, 2003, **42**, 5348–5356.
26 A. Chaumont and G. Wipff, *Inorg. Chem.*, 2004, **43**, 5891–5901.
27 A. Chaumont and G. Wipff, *Chem.–Eur. J.*, 2004, **10**, 3919–3930.
28 A. Chaumont and G. Wipff, *J. Phys. Chem. B*, 2004, **108**, 3311–3319.
29 A. Chaumont and G. Wipff, *Phys. Chem. Chem. Phys.*, 2005, **7**, 1926–1932.
30 C. G. Hanke, N. A. Atamas and R. M. Lynden-Bell, *Green Chem.*, 2002, **4**, 107–111.
31 C. G. Hanke, A. Johansson, J. B. Harper and R. M. Lynden-Bell, *Chem. Phys. Lett.*, 2003, **374**, 85–90.
32 C. G. Hanke and R. M. Lynden-Bell, *J. Phys. Chem. B*, 2003, **107**, 10873–10878.
33 J. K. Shah and E. J. Maginn, *J. Phys. Chem. B*, 2005, **109**, 10395–10405.
34 C. Cadena, J. L. Anthony, J. K. Shah, T. I. Morrow, J. F. Brennecke and E. J. Maginn, *J. Am. Chem. Soc.*, 2004, 126.
35 V. Halka, T. Tsekov and W. Freyland, *Phys. Chem. Chem. Phys.*, 2005, **7**, 2038–2043.
36 T. Yan, S. Li, W. Jiang, X. Gao, B. Xiang and G. A. Voth, *J. Phys. Chem. B*, 2006, **110**, 1800–1806.
37 R. M. Lynden-Bell and M. Del Popolo, *Phys. Chem. Chem. phys.*, 2006, **8**, 949–954.
38 R. M. Lynden-Bell, J. Kohanoff and M. G. Del Popolo, *Faraday Discuss.*, 2005, **129**, 1–11.
39 A. Chaumont, R. Schurhammer and G. Wipff, *J. Phys. Chem. B*, 2005, **109**, 18964–18973.
40 P. Vayssière, A. Chaumont and G. Wipff, *Phys. Chem. Chem. Phys.*, 2004, **7**, 124–135.
41 N. Sieffert and G. Wipff, *J. Phys. Chem. B*, 2006, **110**, 13076–13085.
42 W. L. Jorgensen, J. Chandrasekhar, J. D. Madura, R. W. Impey and M. L. Klein, *J. Phys. Chem.*, 1983, **79**, 926.
43 H. J. C. Berendsen, J. R. Grigera and T. P. Straatsma, *J. Phys. Chem.*, 1987, **91**, 6269–6271.
44 M. W. Mahoney and W. L. Jorgensen, *J. Chem. Phys.*, 2000, **112**, 8910–8922.
45 M. W. Mahoney and W. L. Jorgensen, *J. Chem. Phys.*, 2001, **114**, 363–366.
46 D. A. Case, D. A. Pearlman, J. W. Cadwell, T. E. Cheatham III, J. Wang, W. S. Ross, C. L. Simmerling, T. A. Darden, K. M. Merz, R. V. Stanton, A. L. Cheng, J. J. Vincent, M. Crowley, V. Tsui, H. Gohlke, R. J. Radmer, Y. Duan, J. Pitera, I. Massova, G. L. Seibel, U. C. Singh, P. K. Weiner and P. A. Kollman, *AMBER7*, University of California, San Francisco, 2002.
47 T. A. Darden, D. M. York and L. G. Pedersen, *J. Chem. Phys.*, 1993, **98**, 10089.
48 G. A. Kaminski and W. L. Jorgensen, *J. Chem. Soc., Perkin Trans. 2*, 1999, 2365–2375.
49 J. de Andrade, E. S. Boes and H. Stassen, *J. Phys. Chem. B*, 2002, **106**, 13344–13351.
50 W. D. Cornell, P. Cieplak, C. I. Bayly, I. R. Gould, K. M. Merz, D. M. Ferguson, D. C. Spellmeyer, T. Fox, J. W. Caldwell and P. A. Kollman, *J. Am. Chem. Soc.*, 1995, **117**, 5179–5197.
51 H. J. C. Berendsen, J. P. M. Postma, W. F. van Gunsteren and A. Di Nola, *J. Chem. Phys.*, 1984, **81**, 3684.
52 Y. Duan, S. Kumar, J. M. Rosenberg and P. A. Kollman, *J. Comput. Chem.*, 1995, **16**, 1351–1356.
53 E. Engler and G. Wipff, in *Crystallography of Supramolecular Compounds*, ed. G. Tsoucaris, Kluwer, Dordrecht, 1996, pp. 471–476.
54 W. Humphrey, A. Dalke and K. Schulten, *J. Mol. Graphics*, 1996, **14**, 33–38.
55 H. Luo and P. V. Bonnesen, *Anal. Chem.*, 2004, **76**, 2773–2779.
56 J. Jacquemin, P. Husson, A. A. H. Padua and V. Majer, *Green Chem.*, 2006, **8**, 172–180.
57 U. Schröder, J. D. Wadhawan, R. G. Compton, F. Marken, P. A. Z. Suarez, C. S. Consorti, R. F. de Souza and J. Dupont, *New J. Chem.*, 2000, **24**, 1009–1015.
58 N. Muzet, E. Engler and G. Wipff, *J. Phys. Chem. B*, 1998, **102**, 10772–10788.
59 G. Wipff, E. Engler, P. Guilbaud, M. Lauterbach, L. Troxler and A. Varnek, *New J. Chem.*, 1996, **20**, 403–417.
60 S. E. Feller, R. W. Pastor, A. Rojnuckarin, S. Bogusz and B. R. Brooks, *J. Phys. Chem.*, 1996, **100**, 17011–17020.
61 S. L. I. Toh, J. McFarlane, C. Tsouris, D. W. DePaoli, H. Luo and S. Dai, *Solvent Extr. Ion Exch.*, 2006, **24**, 33–36.

